

Stochastic Electrical Detection of Single Ion-Gated Semiconducting Polymers

Ab F. Nieuwenhuis, Daniel F. Duarte Sánchez, Jin Z. Cui, and Serge G. Lemay*

Semiconducting polymer chains constitute the building blocks for a wide range of electronic materials and devices. However, most of their electrical characteristics at the single-molecule level have received little attention. Elucidating these properties can help understanding performance limits and enable new applications. Here, coupled ionic–electronic charge transport is exploited to measure the quasi-1D electrical current through long single conjugated polymer chains as they form transient contacts with electrodes separated by ≈ 10 nm. Fluctuations between internal conformations of the individual polymers are resolved as abrupt, multilevel switches in the electrical current. This behavior is consistent with the theoretical simulations based on the worm-like-chain (WLC) model for semiflexible polymers. In addition to probing the intrinsic properties of single semiconducting polymer chains, the results provide an unprecedented window into the dynamics of random-coil polymers and enable the use of semiconducting polymers as electrical labels for single-molecule (bio)sensing assays.

or gated—via the electrostatic potential of the liquid. When the polymer film is impermeable to electrolyte ions, applying such a gate potential forms an electrical double layer (EDL) at the film surface. The EDL consists of a thin charged ionic sheet on the electrolyte side that is compensated by a quasi-2D layer of electrons or holes at the surface of the semiconductor (Figure 1a), resulting in conventional OFET operation. The charge carrier density achieved by liquid gating is significantly higher than in conventional FETs because of the high capacitance of the EDL ($1\text{--}10\ \mu\text{F cm}^{-2}$). When the semiconductor is permeable to ions, on the other hand, an accumulation-type OECT is formed.^[13] Here ions infiltrate the 3D bulk of the semiconductor where they induce electrons or holes so as to maintain charge neutrality (Figure 1b). Because of this penetration, the effective gate capacitance of OECTs can be as high as

$10\text{--}100\ \mu\text{F cm}^{-2}$.^[14] The transport properties of single polymer chains in electrolyte represent the convergence between OFET and OECT modes of operation: the single polymer chain is electrostatically doped by a well-defined EDL, as in an OFET, yet it is simultaneously permeated by ions due to its open coil structure, as in an OECT (Figure 1c).^[15] Contrary to both OFETs and OECTs, where hopping between polymer chains plays an important role, here transport can occur primarily along the backbone of the polymer in a quasi-1D fashion.


Our approach for interrogating single polymers is sketched in Figure 1d,e. We employ pairs of electrodes separated by a ≈ 10 nm-thick insulator layer to form a vertical OFET (VOFET^[16–18]) and immerse this structure in an inert electrolyte. The electrode–insulator–electrode nanogap geometry is readily achieved in microfabricated devices by carefully controlling the thickness of an insulating layer and using the top electrode as a mask in a self-aligned process.^[19] The resulting open architecture allows exposing the electrodes to a solution in which polymers undergoing Brownian motion can intermittently make contact with the drain and/or the source electrode. Through the action of the potential applied to a reference electrode immersed in the solution and acting as a gate, the molecules become p-doped and enter their conducting state upon contact.^[20] The temporary conducting pathway thus created between the source and drain is detected amperometrically via a small potential difference

1. Introduction

Semiconducting polymers are fascinating electronic materials and key to rapidly evolving technologies including organic electronics,^[1] solar cells,^[2] and light-emitting diodes.^[3] Probing the transport properties of their fundamental building blocks—single polymer chains—has however proven remarkably challenging,^[4] despite early successes for short oligos based on scanning tunneling microscopy,^[5–7] guided assembly,^[8] and electrodeposition.^[9–11] Here, we explore single-polymer-chain transport properties using coupled ionic–electronic charge transport, a technique for controlling the conductance in organic field-effect transistors (OFET) and organic electrochemical transistors (OECTs).^[12]

The conductance of a semiconducting conjugated polymer thin film in contact with a liquid electrolyte can be modulated—

A. F. Nieuwenhuis, D. F. Duarte Sánchez, J. Z. Cui, S. G. Lemay
University of Twente
Drienerloaan 5, Enschede 7522 NB, Netherlands
E-mail: s.g.lemay@utwente.nl

 The ORCID identification number(s) for the author(s) of this article can be found under <https://doi.org/10.1002/adma.202307912>

© 2023 The Authors. Advanced Materials published by Wiley-VCH GmbH. This is an open access article under the terms of the Creative Commons Attribution License, which permits use, distribution and reproduction in any medium, provided the original work is properly cited.

DOI: 10.1002/adma.202307912

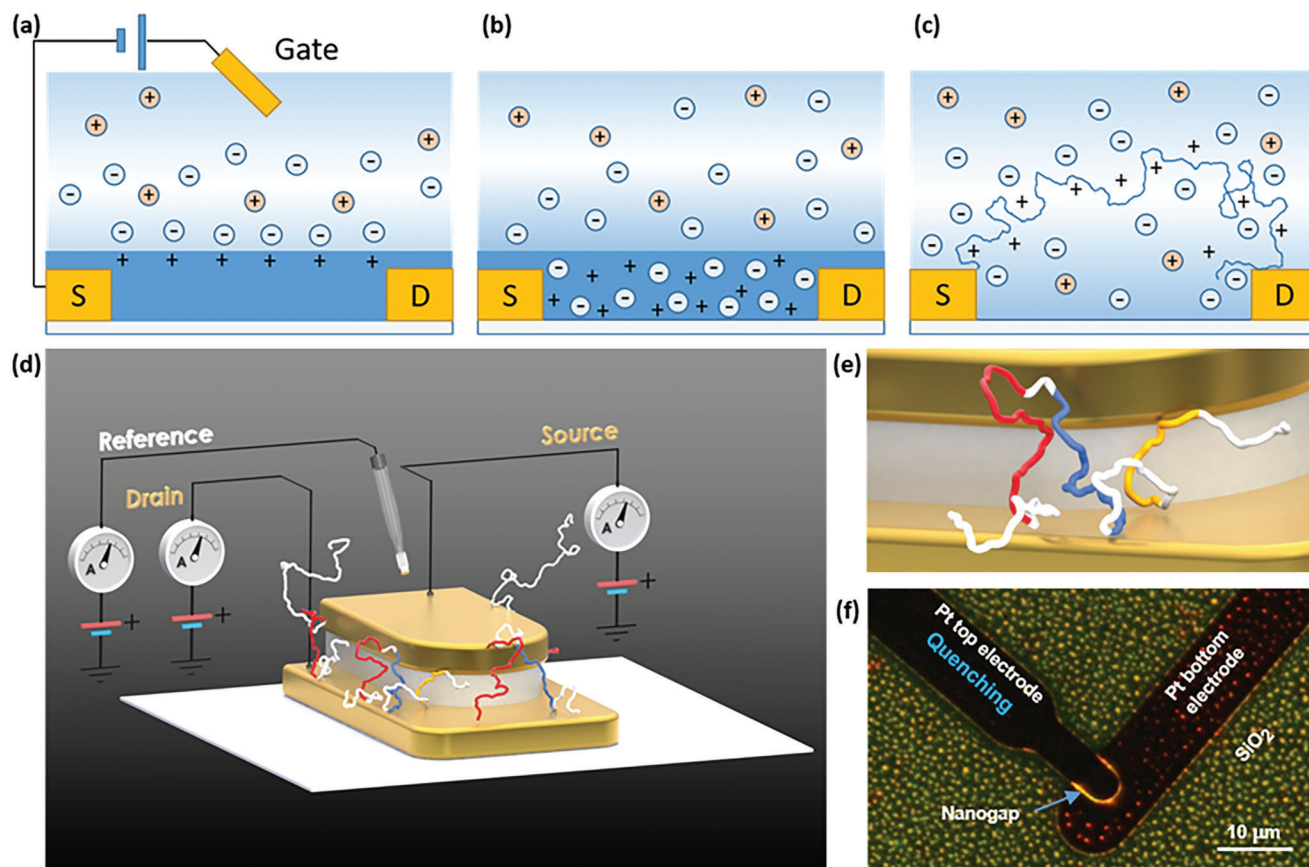


Figure 1. Experimental configuration. a) Schematic illustration of an OFET based on a thin polymer film impermeable to electrolyte ions. Applying a gate potential induces an EDL consisting of ions in the solution and compensating charge carriers (here shown as holes) in the semiconductor. b) An accumulation-type OECT permeable to electrolyte ions. Infiltrating ions accumulate in the bulk of the semiconductor, where they induce electronic charge carriers to maintain charge neutrality. c) A single polymer chain electrostatically doped by a well-defined EDL and simultaneously penetrated by ions due to its open structure. d) Sketch of our electrochemically gated experimental configuration. An electrical current flows between two electrodes separated by a thin insulator when they are connected by a polymer coil. The hole density in the polymer is controlled by the electrostatic potential of the solution, which is set via a reference (gate) electrode. We monitored the current at all three electrodes to disentangle the contributions from polymer conduction, electrochemical reactions, and any eventual parasitic leakage. e) Expanded illustration of a polymer configuration forming three distinct conductive pathways between the drain and source electrode (red, blue, and yellow). f) Photoluminescence from polymers that were drop cast from a high (μm) concentration solution. Visible are the bottom electrode (top right), the top electrode (top left), and the overlap region where a nanogap geometry is formed. Polymers adsorbed to both the Pt electrodes (red spots) and the surrounding SiO_2 substrate (yellow spots). The change in color is attributed to quenching of photoluminescence by Pt.^[24] Bright yellow emission is also visible from polymers adsorbed to the insulating silicon nitride spacer between the electrodes (white region in Figure 1e). The density of spots was approximately uniform, suggesting a comparable propensity for adsorption on both electrodes and substrate.

(20 mV) symmetrically applied between the source and drain electrodes.

As a prototypical system, we used regio-regular poly(3-butylthiophene-2,5-diyl) (P3BT). The polymer was first solvated in chloroform, then mixed with tetrabutylammonium perchlorate (TBAP) in acetonitrile (ACN) as a supporting electrolyte (final salt concentration 2 mM). The individual chains had an average length of ($N_{\text{mer}} = 407$ monomers (contour length 155 nm) and a solvated radius of gyration $R_{\text{hyd}} = 4.7$ nm (Section SI, Supporting Information). This is larger than expected for a close-packed chain (2.6 nm based on bulk density),^[21] indicating an open coil geometry. The size of the coil also matched the spacing between our electrodes, permitting simultaneous contact to both electrodes. P3BT is highly fluorescent,^[22,23] which allows its visualization on the surface of the devices by optical mi-

croscopy (Figure 1f). Fluorescence measurements on polymers deposited at low concentration provided further confirmation that the polymers did not aggregate (Section SII, Supporting Information).

2. Results

Before attempting single-polymer measurements, we first characterized our devices in the classic VOFET configuration. To do so, we exposed the nanogap region to a $5 \mu\text{m}$ solution of P3BT in chloroform mixed with a 20 mM solution of TBAP in ACN in a ratio of 1:4. This high polymer concentration led to the formation of a semiconducting channel between the source and drain electrodes in ≈ 1 h (Figure S4c, Supporting Information). These films were stabilized by refilling the solution volume lost by

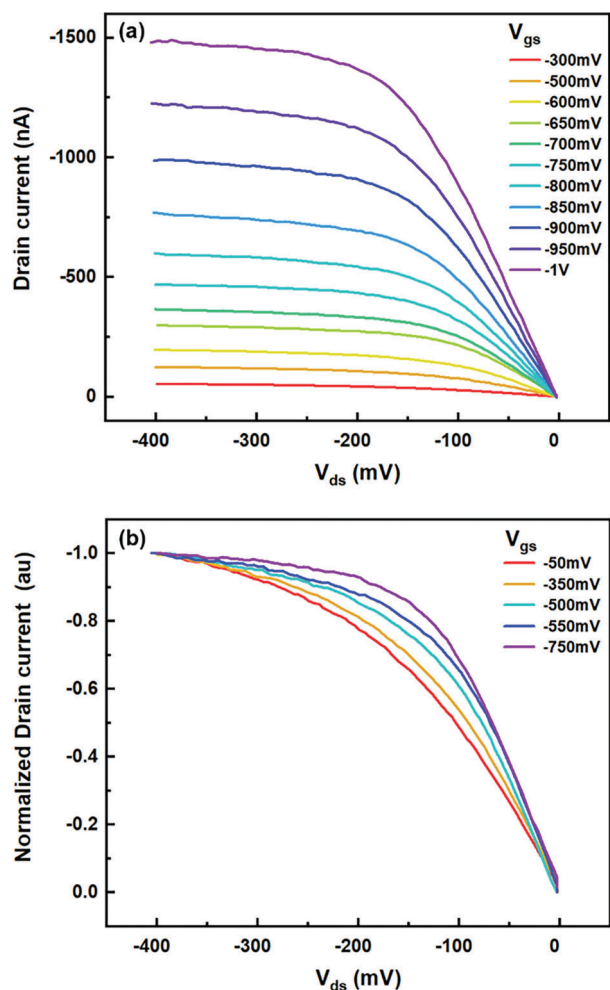


Figure 2. Output characteristics of the VOFET with a channel length of 10 nm. a) Gate-source voltages varied between -300 and -1000 mV. b) Normalized drain currents, gate-source voltages varied between -50 and -750 mV. The channel was formed in ≈ 1 h (adsorption) using a $5 \mu\text{M}$ solution of P3BT in chloroform mixed with a 20 mM solution of TBAP in ACN in a ratio of 1:4. The scan rate of the drain-source voltage was 10 mV s^{-1} .

evaporation with pure ACN in which P3BT is much less soluble. The stable channel allowed us to record the output characteristics of the 10 nm short channel VOFET (Figure 2). In each curve the drain-source voltage was scanned with respect to a fixed gate-source voltage. The drain current rose linearly at low drain-source voltages and saturated at drain-source voltages above pinch-off, as expected (Figure 2a). Saturation became more pronounced with increasing gate-source voltages (Figure 2b). Exposing the electrodes to much lower nM-level polymer concentrations still led to the gradual formation of a semiconducting channel between the electrodes (Section SIII, Supporting Information). In this case, the source-drain current was however smaller by 3 orders of magnitude, comparable to the change in concentration.

The character of the electrical response changed dramatically at lower (100 pM-level) polymer concentrations, however, as il-

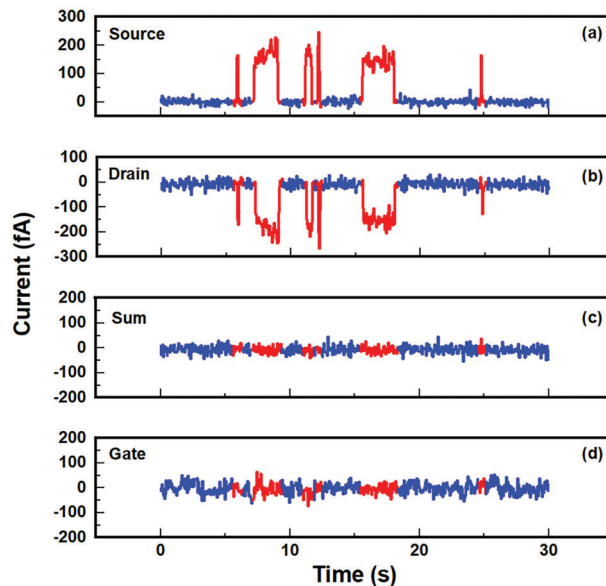


Figure 3. a–c) Amperometric responses at the source (a), drain (b), and gate electrode (d). For clarity, a DC baseline current has been subtracted from each trace. c) Summed amperometric responses of the source and drain electrodes.

lustrated in the amperometric data of Figure 3. Here a constant baseline current was measured at the source electrode during quiescent periods that lasted anywhere from a few seconds to a few minutes. On occasion, the current quickly jumped to a new, approximately constant value of order 100 fA before switching back to the off state a few seconds later (Figure 3a). The drain current simultaneously underwent similar transients with the opposite polarity (Figure 3b). Figure 3c shows that the sum of the source and drain currents was constant apart from the summed noise, indicating that the current transients were fully anticorrelated. This implies that these transients correspond to currents flowing between the source and drain electrodes, presumably due to the presence of polymer material temporarily bridging the electrodes. The simultaneously measured gate current remained constant during the transients (Figure 3d), indicating that any current resulting from polymer oxidation or reduction remained undetectably small. The current noise at the gate electrode was somewhat higher than the summed current noise in Figure 3c; this was caused by unused nanogaps on the same chip that were also exposed to the electrolyte-polymer solution.

The temporal evolution of the stochastic signals exhibited a broad range of behaviors. In the simplest instances, single pulses were observed, as illustrated in Figure 4a. In other instances (Figures 3 and 4b), multiple consecutive telegraph-like switches between the conducting and non-conducting states were observed instead. More complex events were also regularly recorded involving multiple, well-defined current plateaus, as shown in Figure 4c,d.

We attribute these abrupt, reversible changes in the current to individual polymer molecules temporarily bridging the two electrodes. Considering the observed current levels and assuming a uniform longitudinal electric field along the single-molecule channel, we estimate the charge carrier mobility to be in the 10^{-7}

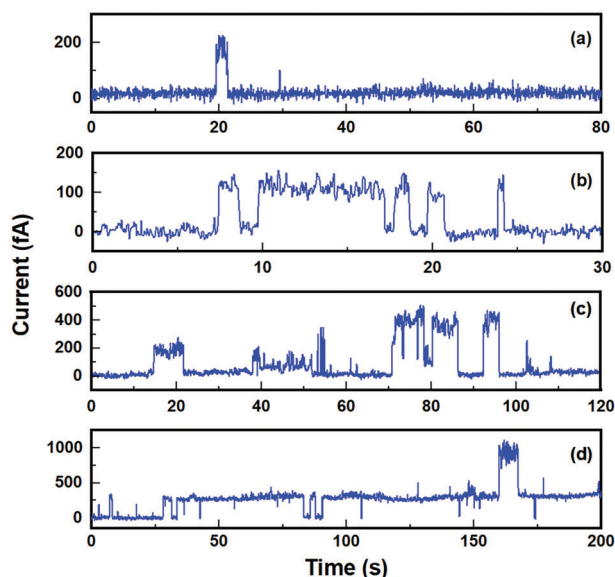


Figure 4. Amperometric response (source current) from single polymer molecules. These typical current-time traces are organized in order of increasing complexity. a) Single-plateau event. b) Telegraph-like signal consisting of a train of similarly-sized plateaus. c, d) Events exhibiting multiple current levels.

to $10^{-5} \text{ cm}^2 \text{ V}^{-1} \text{ s}^{-1}$ range, which is consistent with values reported for highly amorphous polythiophene films^[25,26] (Section SVI, Supporting Information). We attribute the multilevel current fluctuations to variations in the internal conformation of a single polymer caused by Brownian motion. This can be expected since the polymer contour length ($\approx 155 \text{ nm}$) is much longer than the electrode spacing ($\approx 10 \text{ nm}$), allowing the formation of multiple contacts. While the participation of more than one molecule can never be excluded entirely in any given amperometric trace, the long quiet periods interspersed with bursts of complex activity are incompatible with a scenario where multilevel fluctuations are predominantly caused by multiple molecules (Section SIV, Supporting Information). This configuration-driven switching mechanism at constant potential is also conceptually distinct from the redox mechanism proposed earlier to explain voltage-dependent switching in surface-polymerized molecular bridges or short anchored molecules.^[9,27]

The telegraph-like current fluctuations occurred on a time scale of seconds, which is far too long to represent the conformational fluctuations of a fully solvated chain. For comparison, the Rouse time for polymer relaxation is $\approx 4 \mu\text{s}$ for our molecules,^[28] five orders of magnitude shorter than our observed events. These slow dynamics are consistent with the molecules being reversibly adsorbed on the surface, slowing their diffusion and permitting the observation of extended, relatively stable current plateaus. Based on the fluorescence data (Figure 1f), we infer that this adsorption can take place on both the electrodes as well as the SiN surface between them. On the other hand, the observed time for switching between two plateaus is limited by our transimpedance amplifier rise time of 17 ms. We therefore do not resolve the dynamics during the establishment of contact, as discussed further in Section SVII (Supporting Information).

The question arises as to the extent to which the observed behavior is dictated by contact resistance. Many reported OFETs with sub-micrometer channels lengths show deteriorated output characteristics referred to as short-channel behavior. This is characterized by an absent or strongly tilted saturation region in the output curves.^[17,18,29] OFETs suffer from short-channel behavior when the contact resistances become comparable to the channel resistance. This is often attributed to an injection barrier (Schottky barrier,^[30] or Fermi-level pinning^[31,32]) at the polymer-electrode interface. An advantage of our ion-gated configuration is that contact resistance is not expected to be significant.^[33,34] The mobile ions in solution provide a high degree of screening (Debye length $\approx 2.2 \text{ nm}$), making the transversal electric field induced by the gate electrode much higher than the longitudinal field along the channel. This is known to suppress the formation of injection barriers at the polymer-electrode interface.^[33,35] Indeed, the output characteristics at higher gate-source voltages (Figure 2a) do not exhibit short channel behavior. At less negative gate-source voltages, the output curves beyond pinch off become slightly tilted despite higher channel resistance. This is clearest in Figure 2b, which shows normalized drain currents. The transverse electric field at these low gate-source voltages is then insufficient to fully suppress short-channel effects. The short-channel effects are nonetheless greatly reduced and comparable with the behavior observed in long-channel OFETs.^[29] Additionally, we regularly observed very slow fluctuations in the current of otherwise stable long plateaus, as illustrated in Figure 4d. This can be interpreted as slow variations in the length of the conducting pathway(s) as the polymer rearranges itself between the electrodes. This again suggests that transport along the backbone, as opposed to the contacts, dominates the overall device resistance.

3. Discussion

To elucidate the origin of the current fluctuations, we first performed an autocorrelation analysis on long amperometric traces. As seen in Figure 5a, the autocorrelation function (ACF) (Section SVIII, Supporting Information) has the form $\text{ACF}(\tau) \sim C - \ln(\tau)$ with C a constant and τ the time delay or lag. This indicates that the abrupt switching events do not have a characteristic time scale and instead exhibit a broad range of relaxation times. Analyzing the corresponding power spectrum of the current fluctuations provides further evidence for a mechanism distinct from conventional low-frequency electronic noise. Figure 5b shows the current noise power spectral density (PSD) ($S_I(f)$) at different values of the average current ($\langle I \rangle$) corresponding to different amounts of adsorbed polymers (Section SIX, Supporting Information). The spectrum has the form $S_I(f) \propto f^{-\beta}$ with β ranging from 0.83 to 1.13. Such $1/f$ noise, also known as flicker or pink noise, is ubiquitous in electrical conductors.^[36] The logarithmic form for the ACF in Figure 5a is consistent with a stationary stochastic process with this spectrum.^[37] $1/f$ noise is commonly described in terms of Hooge's empirical model,

$$\frac{S_I(f)}{\langle I \rangle^2} = \frac{\alpha_H}{N_C f^\beta} \quad (1)$$

with N_C the number of charge carriers and α_H an empirical constant.^[38] We estimate from the measurement at the

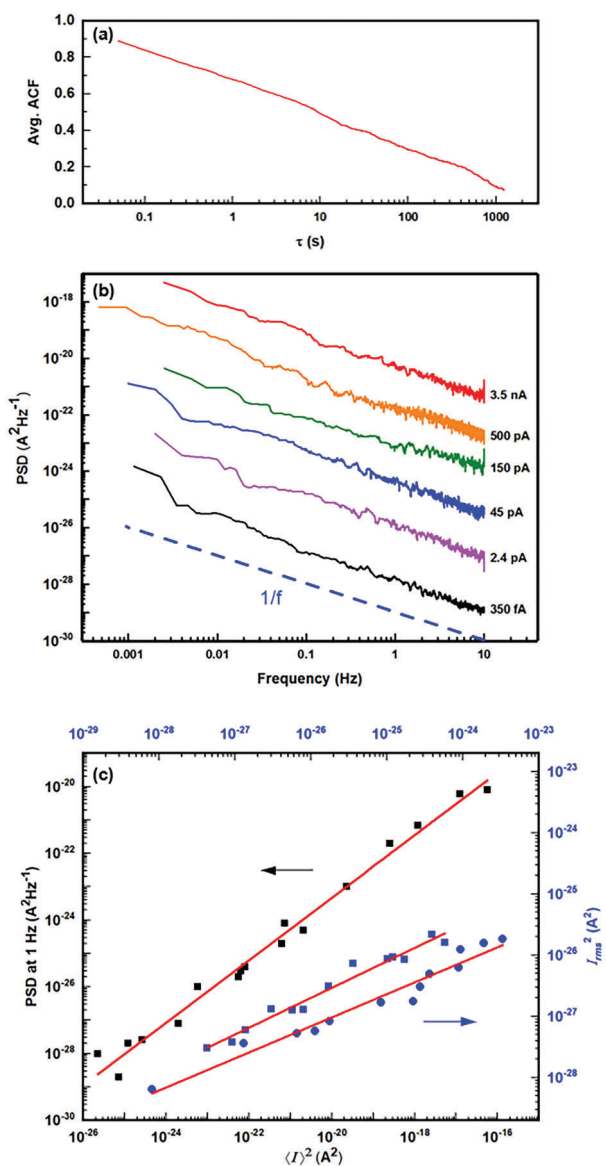


Figure 5. Dynamical properties. a) Autocorrelation function of an amperometric trace. The correlation decays linearly with $\log \tau$, where τ is the time delay, indicating a broad distribution of relaxation times. b) PSD for different average current levels spanning four orders of magnitude. In each case, the PSD exhibits a $1/f$ -like behavior. c) PSD at 1 Hz for complete traces (black squares) and mean square current noise I_{rms}^2 on current plateaus (blue symbols) vs $\langle I \rangle^2$. The noise scales differently with current for the complete traces (red line, slope 0.94 ± 0.03) and on the plateaus (slopes 0.53 ± 0.03 and 0.60 ± 0.03 for qualitative and automated determination methods, respectively, as described in Section SXI, Supporting Information).

lowest current level (350 fA) that $\alpha_{\text{H}} \approx 0.02$ (Section SX, Supporting Information), which falls within the broad range of values reported for disordered organic conductors (0.01–20).^[39,40] Figure 5c (black squares) however shows that the measured PSD scales essentially linearly with $\langle I \rangle^2$. According to Equation (1), this would imply that the number of charge carriers N_{C} remains constant even as the current increases by four or

orders of magnitude due to the accumulation of additional material between the electrodes, an implausible scenario. In contrast, we also evaluated the rms noise current, I_{rms} , within individual, stable plateaus exhibiting no switching events (Section SXI, Supporting Information). Figure 4c (blue symbols) shows that, to a very good approximation, $I_{\text{rms}} \propto \langle I \rangle^{1/2}$ within these plateaus. This behavior agrees with the Hooge model under the assumption that $\langle I \rangle \propto N_{\text{C}}$ and is consistent with changes in $\langle I \rangle$ being regulated by the amount of polymer material between the electrodes. Noise on each current plateau thus behaves as in conventional (semi)conductors, but the overall spectrum is dominated by excess noise with a different origin. This supports the interpretation that the plateaus correspond to configurations where the polymers behave as stable wires, as also occurs in thin films, whereas the abrupt switches and excess noise correspond to rearrangements of the polymer conformation exhibiting different conductive pathways between the electrodes (Figure 1d).

To gain further insight into these conformational fluctuations, we employed a Monte Carlo method based on the 2D worm-like chain (WLC) polymer model (Section SXII, Supporting Information).^[41,42] Figure 6 shows typical examples of random adsorbed polymer configurations ranging from compact (a) to somewhat extended (b) and highly extended (c). While extended configurations can span electrodes with a larger spacing, compact configurations instead provide more conduction pathways between closely spaced electrodes.

Based on the simulations, we determined the number of conducting pathways between two electrodes for 5000 randomly generated polymer configurations. The position of the electrodes was scanned relative to each polymer configuration to account for translation along the surface (Figure 6d). Figure 6e shows histograms of the relative probability of finding a particular number of pathways as a function of nanogap size. For a 10 nm gap electrode spacing, the number of conducting paths is limited to 4 or fewer. The average number of pathways increases slightly from 1.4 for 10 nm gaps to 1.9 for 5 nm gaps, and the probability of finding n conducting pathways decreases exponentially with n (Figure 6e). Figure 6f shows the corresponding distributions of simulated path lengths for the different gap sizes. The conducting pathway lengths exhibit a broad distribution, consistent with the experimentally observed variations in plateau conductance (the experimental plateaus are however too short to explore the full distribution within a single plateau). Not unexpectedly, smaller gaps favor shorter pathways: the average path length decreases from 25 nm for 10 nm gaps to 10 nm for the smallest 5 nm gaps. Importantly, the model predicts that only a few conducting paths can be expected for each individual polymer molecule, consistent with the typical number of plateaus typically observed in the amperometric measurements. This further supports the hypothesis that the observed switching behavior is due to rearrangements of the polymer configuration due to Brownian motion.

4. Conclusion

Our experiments demonstrate that individual semiconducting polymer chains can be electrically addressed while in a random coil configuration using mixed ionic and electronic transport. This allows probing the electrical properties of individual

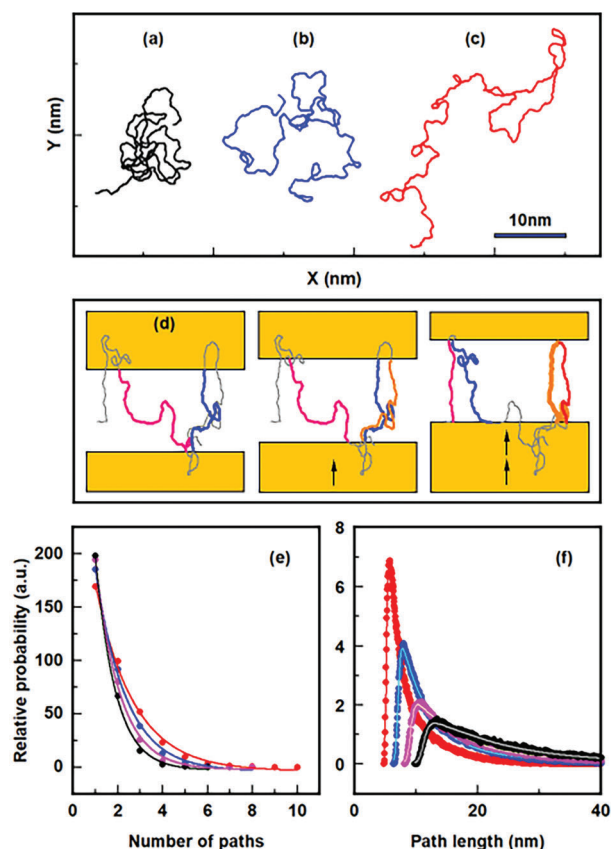


Figure 6. WLC model. a–c) Typical examples of polymer configurations from the 2D WLC model. Shown are: a) compact, b) somewhat extended, and c) highly extended configurations. d) 5000 random configurations were generated and for each the number and length of pathways were determined for different relative positions of the electrodes (electrodes shifted in increments of 0.38 nm). Here this process is illustrated for one particular polymer configuration exhibiting 2, 3, or 4 conducting pathways depending on the position of the electrodes. Since the polymers are adsorbed to the surface, the 3D geometry of the device was simplified to a 2D geometry in which the electrodes and the gap in between are coplanar. e) Distribution of the number of conducting paths for gap sizes of 10 nm (black), 8.3 nm (purple), 6.7 nm (blue), and 5 nm (red). The solid lines are exponential fits. f) Corresponding distributions of the path length. The solid lines are fits to the biphasic Hill equation (Section SXII, Supporting Information).

molecules. Surprisingly, it also permits observing their otherwise inaccessible internal conformation fluctuations. We envision that our approach can be further extended by ligating semiconducting polymers to analytically relevant receptors such as nucleic acids and antibodies. Doing so will turn the polymers into the electrical equivalent of fluorescent labels for a new class of single-entity (bio)sensing assays based on all-electrical signal transduction.

5. Experimental Section

Chemicals: P3BT regioregular electronic grade was purchased from Rieke Metals (cat. no. 4001-E), TBAP from Fluka (cat. no. 689350g), ACN (for HPLC $\geq 99.9\%$) from Sigma–Aldrich (cat. no. 3449181L), chloroform (anhydrous $\geq 99\%$) from Sigma–Aldrich (cat. no. 2883061L), 2-propanol

(for HPLC 99.9%) from Sigma–Aldrich (cat. no. 348632.5LM), and acetone ($\geq 99.5\%$ GC) from Sigma–Aldrich (cat. no. 322012.5LM). All chemicals were used as received.

P3BT was originally dissolved in chloroform. 20 mM TBAP in ACN was mixed with the chloroform solution in a 1:9 ratio to form the supporting electrolyte (final salt concentration 2 mM). Syringe filters with pore size 0.2 μm (Whatman SPARTAN RC 30) were used to remove most of the remaining undissolved polymers or contaminants. As a result of filtering, the actual polymer concentration may be lower than the nominal concentration.

Dynamic Light Scattering: Dynamic light scattering (DLS) measurements were carried out with a Malvern Zetasizer Nano ZS instrument equipped with a 633 nm laser set at an angle of 173°. Analysis was performed using software provided by the manufacturer (Zetasizer Software, Malvern).

Fluorescence Microscopy: Light emitted from photoexcited polymers was recorded with a reflex camera (Pentax, model K5) and a fluorescence microscope (Zeiss, Axio Scope Vario). The excitation wavelength was between 450 and 490 nm using Zeiss Filter set 09.

Nanogap Electrode Fabrication: Lithographically fabricated nanogap electrodes were employed with an open architecture. The nanogaps consisted of a pair of Pt thin-film electrodes separated by a thin, low-stress silicon nitride insulating dielectric layer, as sketched in Figure 1. The process flow for fabricating these devices is described in Section SXIII (Supporting Information).

Electrochemical Measurements: Prior to experiments, the chips were consecutively cleaned ultrasonically in acetone and 2-propanol at 50 °C. The clean chips were placed in a custom-made socket (Section SXIV, Supporting Information) and connected to transimpedance amplifiers (Femto DDCPA-300) operating as source meters. A positive current corresponded to current injected into the cell for all three electrodes. The resistance of each nanogap was measured in the dry state by applying a small voltage (20–100 mV) across the nanogap to ensure leakage currents were negligible (< 100 fA). Occasionally the device resistance fluctuated resulting in small anti-correlated currents (tens of fA). These devices were excluded to ensure that anticorrelated currents in measurements were solely due to polymers spanning the gap electrodes. A poly(dimethylsiloxane) (PDMS) reservoir was positioned on top of the chips and filled with the electrolyte solution without polymers. The source and drain electrodes were biased at ± 10 mV with respect to circuit ground. A Pt wire inserted into the fluid was biased at -500 mV and served as a liquid gate electrode. This was sufficient to cause P3BT to become oxidized (p-doped) upon establishing an electrical contact with either of the electrodes since the onset of oxidation occurs at a gate potential of ca. -200 mV. While a more negative gate potential would yield a higher source–drain current, which would improve the signal-to-noise ratio, it was observed that at these potentials the events became shorter and ultimately undetectable, presumably due to desorption. It was first checked that no switching events took place over a period of at least 10 min in the presence of supporting electrolyte only. Finally, the polymer solution was added to the electrolyte in a 1:9 ratio and the subsequent current-time response was observed. The source, drain, and gate currents were monitored separately. Any gate current resulting from polymer oxidation was undetectably small at the low concentrations employed here while the source and drain currents had the same magnitude but opposite signs, as described in the main text. We refer to this current as the source–drain current.

Control Measurements: Section SV (Supporting Information) describes control measurements for electrolyte solutions without polymers to exclude features not related to conducting polymer molecules, and measurements on P3BT, poly(3-hexylthiophene-2,5-diyl) (P3HT), and poly(3-octylthiophene-2,5-diyl) (P3OT) polymers to show that the experiment is robust enough to discriminate between slightly different molecules.

Supporting Information

Supporting Information is available from the Wiley Online Library or from the author.

Acknowledgements

The authors are grateful to Reinder Coehoorn, Peter A. Bobbert, René A. J. Janssen, Cees Otto, Mark Hempenius, Annemarie Huijser, and Stephen Turner for useful discussions, and to Pieter J. Leenaers for carrying out the GPC measurements. This publication was made possible in part by Grant number 1R01HG006882 from National Institutes of Health (NIH); its contents are solely the responsibility of the authors and do not necessarily represent the official views of NIH. Additional financial support was provided by the SENTINEL network, funded by the European Union's Horizon 2020 Research and Innovation Program under Marie Skłodowska-Curie grant agreement no. 812398.

Conflict of Interest

The authors declare no conflict of interest.

Author Contributions

A.F.N. and S.G.L. designed the experiments, and A.F.N. and D.F.D.S. performed them. J.Z.C. fabricated the devices. A.F.N. and D.F.D.S. processed the experimental data for the manuscript. All authors contributed to the interpretation of the results and assisted in writing the manuscript.

Data Availability Statement

The data that support the findings of this study are openly available in 4TU.ResearchData at <https://doi.org/10.4121/933b3ca9-ed9e-468c-bfcb-217ea3c194a7>.

Keywords

organic electrochemical transistors, organic field-effect transistors, polythiophene, semiconducting polymers, single molecules

Received: August 6, 2023

Published online: October 18, 2023

- [1] C. Wang, H. Dong, W. Hu, Y. Liu, D. Zhu, *Chem. Rev.* **2012**, *112*, 2208.
- [2] G. Li, R. Zhu, Y. Yang, *Nat. Photonics* **2012**, *6*, 153.
- [3] N. Thejo Kalyani, S. J. Dhoble, *Renewable Sustainable Energy Rev.* **2012**, *16*, 2696.
- [4] Z.-Y. Zhang, T. Li, *Chin. Chem. Lett.* **2016**, *27*, 1209.
- [5] L. Lafferentz, F. Ample, H. Yu, S. Hecht, C. Joachim, L. Grill, *Science* **2009**, *323*, 1193.
- [6] G. Reece, H. Bulou, F. Scheurer, V. Speisser, F. Mathevet, C. González, Y. J. Dappe, G. Schull, *J. Phys. Chem. Lett.* **2015**, *6*, 2987.
- [7] G. Kuang, S.-Z. Chen, W. Wang, T. Lin, K. Chen, X. Shang, P. N. Liu, N. Lin, *J. Am. Chem. Soc.* **2016**, *138*, 11140.
- [8] W. Hu, J. Jiang, H. Nakashima, Y. Luo, Y. Kashimura, K.-Q. Chen, Z. Shuai, K. Furukawa, W. Lu, Y. Liu, D. Zhu, K. Torimitsu, *Phys. Rev. Lett.* **2006**, *96*, 027801.
- [9] H. X. He, X. L. Li, N. J. Tao, L. A. Nagahara, I. Amlani, R. Tsui, *Phys. Rev. B* **2003**, *68*, 045302.
- [10] M. Janin, J. Ghilane, J.-C. Lacroix, *J. Am. Chem. Soc.* **2013**, *135*, 2108.
- [11] Y. Ai, J.-C. Lacroix, *Electrochem. Commun.* **2020**, *112*, 106674.
- [12] B. D. Paulsen, K. Tybrandt, E. Stavrinidou, J. Rivnay, *Nat. Mater.* **2020**, *19*, 13.
- [13] J. Rivnay, S. Inal, A. Salleo, R. M. Owens, M. Berggren, G. G. Malliaras, *Nat. Rev. Mater.* **2018**, *3*, 17086.
- [14] D. Rawlings, E. M. Thomas, R. A. Segalman, M. L. Chabynyc, *Chem. Mater.* **2019**, *31*, 8820.
- [15] J. D. Yuen, A. S. Dhoot, E. B. Namdas, N. E. Coates, M. Heeney, I. McCulloch, D. Moses, A. J. Heeger, *J. Am. Chem. Soc.* **2007**, *129*, 14367.
- [16] J. Lenz, F. Del Giudice, F. R. Geisenhof, F. Winterer, R. T. Weitz, *Nat. Nanotechnol.* **2019**, *14*, 579.
- [17] J. Liu, L. Herlogsson, A. Sawatdee, P. Favia, M. Sandberg, X. Crispin, I. Engquist, M. Berggren, *Appl. Phys. Lett.* **2010**, *97*, 103303.
- [18] J. Lenz, A. M. Seiler, F. R. Geisenhof, F. Winterer, K. Watanabe, T. Taniguchi, R. T. Weitz, *Nano Lett.* **2021**, *21*, 4430.
- [19] S. Roy, X. Chen, M.-H. Li, Y. Peng, F. Anariba, Z. Gao, *J. Am. Chem. Soc.* **2009**, *131*, 12211.
- [20] S.e H. Kim, K. Hong, W. Xie, K. H. Lee, S. Zhang, T. P. Lodge, C. D. Frisbie, *Adv. Mater.* **2013**, *25*, 1822.
- [21] J. Ma, K. Hashimoto, T. Koganezawa, K. Tajima, *Chem. Commun.* **2014**, *50*, 3627.
- [22] S. Cook, A. Furube, R. Katoh, *Energy Environ. Sci.* **2008**, *1*, 294.
- [23] R. A. Cruz, T. Catunda, W. M. Facchinatto, D. T. Balogh, R. M. Faria, *Synth. Met.* **2013**, *163*, 38.
- [24] P. J. Goutam, D. K. Singh, P. K. Iyer, *J. Phys. Chem. C* **2012**, *116*, 8196.
- [25] H. Sirringhaus, P. J. Brown, R. H. Friend, M. M. Nielsen, K. Bechgaard, B. M. W. Langeveld-Voss, A. J. H. Spiering, R. A. J. Janssen, E. W. Meijer, P. Herwig, D. M. De Leeuw, *Nature* **1999**, *401*, 685.
- [26] H. Sirringhaus, N. Tessler, R. H. Friend, *Science* **1998**, *280*, 1741.
- [27] J. He, Q. Fu, S. Lindsay, J. W. Ciszek, J. M. Tour, *J. Am. Chem. Soc.* **2006**, *128*, 14828.
- [28] P. E. Rouse, Jr., *J. Chem. Phys.* **1953**, *21*, 1272.
- [29] L. Herlogsson, Y.-Y. Noh, N. Zhao, X. Crispin, H. Sirringhaus, M. Berggren, *Adv. Mater.* **2008**, *20*, 4708.
- [30] C. Liu, Y. Xu, Y.-Y. Noh, *Mater. Today* **2015**, *18*, 79.
- [31] R. C. Shallcross, T. Stubhan, E. L. Ratcliff, A. Kahn, C. J. Brabec, N. R. Armstrong, *J. Phys. Chem. Lett.* **2015**, *6*, 1303.
- [32] Q. Bao, S. Braun, C. Wang, X. Liu, M. Fahlman, *Adv. Mater. Interfaces* **2019**, *6*, 1800897.
- [33] M. Waldrip, O. D. Jurchescu, D. J. Gundlach, E. G. Bittle, *Adv. Funct. Mater.* **2020**, *30*, 1904576.
- [34] A. F. Paterson, H. Faber, A. Savva, G. Nikiforidis, M. Gedda, T. C. Hidalgo, X. Chen, I. McCulloch, T. D. Anthopoulos, S. Inal, *Adv. Mater.* **2019**, *31*, 1902291.
- [35] D. Braga, M. Ha, W. Xie, C. D. Frisbie, *Appl. Phys. Lett.* **2010**, *97*, 193311.
- [36] M. B. Weissman, *Rev. Mod. Phys.* **1988**, *60*, 537.
- [37] F. N. Hooge, P. A. Bobbert, *Phys. B* **1997**, *239*, 223.
- [38] F. N. Hooge, *Phys. B* **1990**, *162*, 344.
- [39] L. K. J. Vandamme, R. Feyaerts, G. Trefán, C. Detcheverry, *J. Appl. Phys.* **2002**, *91*, 719.
- [40] B. R. Conrad, W. G. Cullen, W. Yan, E. D. Williams, *Appl. Phys. Lett.* **2007**, *91*, 242110.
- [41] K. M. Douglass, *Polymer Cpp* **2021**, <https://pypi.org/project/PolymerCpp> (accessed: May 2021).
- [42] M. Fixman, J. Kovac, *J. Chem. Phys.* **2003**, *58*, 1564.